



# Limited Variation between SARS-CoV-2-Infected Individuals in Domain Specificity and Relative Potency of the Antibody Response against the Spike Glycoprotein

Hanora A. Van Ert,<sup>a</sup> Dana W. Bohan,<sup>a</sup> Kai Rogers,<sup>a</sup> Mohammad Fili,<sup>b</sup> Roberth A. Rojas Chávez,<sup>a</sup>  Enya Qing,<sup>c</sup> Changze Han,<sup>a</sup> Spencer Dempewolf,<sup>a</sup> Guiping Hu,<sup>b</sup> Nathan Schwery,<sup>a</sup> Kristina Sevcik,<sup>a</sup> Natalie Ruggio,<sup>a</sup> Devlin Boyt,<sup>a</sup> Michael A. Pentella,<sup>d</sup>  Tom Gallagher,<sup>c</sup> J. Brooks Jackson,<sup>e</sup> Anna E. Merrill,<sup>e</sup> C. Michael Knudson,<sup>e</sup> Grant D. Brown,<sup>f</sup> Wendy Maury,<sup>a</sup>  Hillel Haim<sup>a</sup>

<sup>a</sup>Department of Microbiology and Immunology, The University of Iowa, Iowa City, Iowa, United States

<sup>b</sup>Department of Industrial and Manufacturing Systems Engineering, Iowa State University, Ames, Iowa, United States

<sup>c</sup>Department of Microbiology and Immunology, Loyola University Chicago, Maywood, Illinois, United States

<sup>d</sup>State Hygienic Laboratory, The University of Iowa, Iowa City, Iowa, United States

<sup>e</sup>Department of Pathology, University of Iowa Hospitals & Clinics, Iowa City, Iowa, United States

<sup>f</sup>Department of Biostatistics, School of Public Health, The University of Iowa, Iowa City, Iowa, United States

**ABSTRACT** The spike protein of severe acute respiratory syndrome coronavirus 2 (SARS-CoV-2) is arranged as a trimer on the virus surface, composed of three S1 and three S2 subunits. Infected and vaccinated individuals generate antibodies against spike, which can neutralize the virus. Most antibodies target the receptor-binding domain (RBD) and N-terminal domain (NTD) of S1; however, antibodies against other regions of spike have also been isolated. The interhost variability in domain specificity and relative neutralization efficacy of the antibodies is still poorly characterized. To this end, we tested serum and plasma samples collected from 85 coronavirus disease 2019 (COVID-19) convalescent subjects. Samples were analyzed using seven immunoassays that employ different domains, subunits, and oligomeric forms of spike to capture the antibodies. Samples were also tested for their neutralization of pseudovirus containing SARS-CoV-2 spike and of replication-competent SARS-CoV-2. While the total amount of anti-spike antibodies produced varied among convalescent subjects, we observed an unexpectedly fixed ratio of RBD- to NTD-targeting antibodies. The relative potency of the response (defined as the measured neutralization efficacy relative to the total level of spike-targeting antibodies) also exhibited limited variation between subjects and was not associated with the overall amount of anti-spike antibodies produced. These studies suggest that host-to-host variation in the polyclonal response elicited against SARS-CoV-2 spike in early pandemic subjects is primarily limited to the quantity of antibodies generated rather than their domain specificity or relative neutralization potency.

**IMPORTANCE** Infection by SARS-CoV-2 elicits antibodies against various domains of the spike protein, including the RBD and NTD of subunit S1 and against subunit S2. The antibody responses of different infected individuals exhibit different efficacies to inactivate (neutralize) the virus. Here, we show that the observed variation in the neutralizing activity of the antibody responses in COVID-19 convalescent subjects is caused by differences in the amounts of antibodies rather than their recognition properties or the potency of their antiviral activity. These findings suggest that COVID-19 vaccine strategies that focus on enhancing the overall level of the antibodies will likely elicit a more uniformly efficacious protective response.

**KEYWORDS** SARS-CoV-2, COVID-19, spike protein, convalescent-phase plasma, antibody neutralization, immunoassay, immunoglobulins, N-terminal domain, receptor-binding domain, adaptive immunity, neutralizing antibodies, spike glycoprotein

**Editor** Biao He, Changchun Veterinary Research Institute

**Copyright** © 2022 Van Ert et al. This is an open-access article distributed under the terms of the [Creative Commons Attribution 4.0 International license](https://creativecommons.org/licenses/by/4.0/).

Address correspondence to Hillel Haim, [Hillel-haim@uiowa.edu](mailto:Hillel-haim@uiowa.edu).

The authors declare no conflict of interest.

**Received** 21 December 2021

**Accepted** 28 December 2021

**Published** 26 January 2022

The spike protein on the surface of severe acute respiratory syndrome coronavirus 2 (SARS-CoV-2) mediates fusion with target cells (1, 2). Spike is synthesized as a precursor protein that is cleaved by furin in the producer cells to generate S1 and S2 subunits (3). These subunits are noncovalently associated on the virus surface, where they form a trimer of heterodimers (4). Furin cleavage primes spike for further processing by the serine protease TMPRSS2 on the plasma membrane or the cysteine protease cathepsin L within the endosome (3, 5, 6). Spike is highly immunogenic in humans and, in infected and vaccinated individuals, readily elicits antibodies that play a critical role in protection (7, 8). Most neutralizing antibodies isolated to date target the receptor-binding domain (RBD) on the S1 subunit (9–15). In addition, multiple neutralizing antibodies that target the N-terminal domain (NTD) of S1 have been isolated (16–18). In contrast, neutralizing antibodies against the C-terminal domain (CTD) of S1 or against the S2 subunit are less frequently elicited (19, 20). The variation between individuals in the domain specificity of the antispikes response and in the relative neutralization efficacy of the antibodies produced remains poorly explored.

To address this question, we quantified the binding specificity of antispikes antibodies in 85 convalescent-phase coronavirus disease 2019 (COVID-19) serum and plasma samples using capture antigens that represent different domains, subunits, and oligomeric forms of spike. A panel of seven in-house and commercial immunoassays that quantify antispikes antibodies was tested, as well as a nucleocapsid-based assay. Antibody content in the samples measured by these assays was compared with their neutralization efficacy for SARS-CoV-2. We observed that different subjects exhibit remarkably similar ratios of RBD- to NTD-targeting antibodies. Interestingly, the relative potency of the convalescent-phase samples (defined as the ratio between neutralization efficacy and the amount of antispikes antibodies measured) was also similar in different individuals and was not associated with the robustness of the response against spike. Our results demonstrate limited host-to-host variation in both spike domain specificity and the relative potency of the antibody response elicited after SARS-CoV-2 infection. Therefore, the observed variation between hosts in the neutralizing activity of their polyclonal response is caused by the quantity of antibodies generated rather than the domains targeted or the relative potency of the antibodies.

## RESULTS

**Strong correlations between results of immunoassays that apply different spike components as the capture antigen.** To determine the target specificity of the SARS-CoV-2 antibody response, we analyzed serum and plasma samples collected from individuals who had recovered from COVID-19 (see all donor information in Data Set S1 in the supplemental material). Serum samples were obtained from individuals willing to donate convalescent-phase plasma for the treatment of COVID-19 patients. In addition, we analyzed plasma samples from obstetric patients who had serologic evidence of COVID-19 infection; samples were collected during their hospitalization for delivery (21). All samples were collected between March 2020 and January 2021. None of the donors required hospitalization for COVID-19-related symptoms. For 68% of donors, the precise date of positivity for SARS-CoV-2 (by PCR analysis of a nasopharyngeal swab) was known; among these subjects, 82% of the serum or plasma samples were collected within 60 days of the positive PCR result (Fig. S1A). For each serum or plasma sample, we quantified the levels of SARS-CoV-2-specific antibodies using commercially available and in-house-developed immunoassays that apply different domains, subunits, or oligomeric forms of the spike protein as the capture antigen (Table 1 and Fig. 1A). To mimic the native spike trimer on the virus surface, we used a cell-based enzyme-linked immunosorbent assay (cbELISA) that measures antibodies against the full-length membrane-bound form of spike (22–24). For this purpose, we used human osteosarcoma (HOS) cells that express on their surface fusion-competent spike trimers by transfection with an expression plasmid that encodes the full-length protein. Samples were also tested by ELISAs, in which recombinant soluble dimeric forms of the RBD, NTD, or the complete ectodomain of S1/S2 (designated Ecto) were used as the capture antigens. The Ecto protein was generated by

**TABLE 1** Immunoassays and capture antigens used in this study

Assay	No. of samples tested (serum, plasma)	Capture antigen used	Assay type	Ig isotype(s) detected <sup>a</sup>
NTD (ELISA)	85 (57, 28)	NTD	In-house ELISA	IgG, IgM, IgA
RBD (ELISA)	85 (57, 28)	RBD	In-house ELISA	IgG, IgM, IgA
Ecto (ELISA)	85 (57, 28)	S1/S2 ectodomain	In-house ELISA	IgG, IgM, IgA
Cell-based ELISA	85 (57, 28)	Full-length S1/S2 trimers	In-house ELISA	IgG, IgM, IgA
TrimericS (DiaSorin)	85 (57, 28)	Trimeric S1/S2 ectodomain	Commercial assay	IgG
Liaison (DiaSorin)	85 (57, 28)	S1/S2 ectodomain	Commercial assay	IgG
Vitros (Ortho)	57 (57, —) <sup>b</sup>	S1	Commercial assay	IgG
Roche	71 (43, 28)	Nucleocapsid	Commercial assay	IgG, IgM, IgA

<sup>a</sup>The secondary antibody used in the NTD, RBD, and Ecto ELISAs and the cell-based ELISA targets the human kappa light chain.

<sup>b</sup>—, the test was performed only with the 57 serum samples due to assay incompatibility with plasma.

abrogating the furin cleavage site at spike positions 682 to 685 (3). Binding of antibodies in serum or plasma to the above antigens was measured using a secondary antibody specific for the human kappa light chain, which detects isotypes IgG, IgM, and IgA. In addition, we tested the samples with commercial immunoassays that detect IgG against the S1 subunit (Ortho Vitros), S1/S2 subunits (DiaSorin Liaison IgG) and a trimeric soluble form of S1/S2 (DiaSorin TrimericS IgG). To quantify non-spike-targeting antibodies elicited against SARS-CoV-2, we used the Roche assay that measures total antibodies against the nucleocapsid protein of SARS-CoV-2. Given that our study focused on quantitative relationships between antibody levels and neutralization efficacies, we excluded from the analyses all samples that were negative for SARS-CoV-2 antibodies in at least 5 of the 8 immunoassays. Our final test set was composed of 85 samples (57 serum and 28 plasma). The Ortho test was performed only with the 57 serum samples due to assay incompatibility with plasma.

The RBD, NTD and Ecto ELISAs as well as cbELISA showed a normal distribution of their  $\log_{10}$ -transformed values (Fig. 1B; also, see the results of a Shapiro-Wilk test of normality in Fig. S1B). The  $\log_{10}$ -transformed values of the Liaison and TrimericS tests were also normally distributed, whereas the Roche test showed no evidence for normality (Fig. S1B and C). We compared values measured in the different assays using the nonparametric Spearman rank test. Strong correlations were observed between values measured in the assays that apply different spike components as the capture antigens, whereas correlations with the nucleocapsid-based Roche assay were less strong (Fig. 1C and Fig. S2). Interestingly, a strong association was observed between the content of antibodies against the nonoverlapping NTD and RBD of spike (Fig. 1D).

Previous studies have suggested that most spike-targeting antibodies elicited after infection or vaccination target the RBD or NTD (25, 26). We used our in-house ELISA system to compare the relative amounts of antibodies that target the RBD and NTD by calculating for each patient the ratio between the values in these assays. First, we verified that equimolar concentrations of the NTD and RBD used for capture in our ELISAs resulted in similar levels of the probes bound to the plates. To this end, we used a horseradish peroxidase-conjugated antibody that binds to the Fc region contained at the C terminus of these probes. As shown in Fig. 1E, equimolar concentrations of the probes resulted in equivalent amounts of probe binding to the ELISA plates. Comparison of the binding efficiency of the patient antibodies to the RBD and NTD probes revealed a mean RBD-to-NTD ratio of 1.8 with a standard deviation of 0.99 (Fig. 1F). The ratio of RBD to NTD antibodies was relatively constant in different subjects, ranging between 1 and 3 in 78% of cases. Only 2% of the samples showed 2-fold or higher binding to the NTD, and only 8% of the samples showed >3-fold-higher binding to the RBD. The proportion of RBD- or NTD-targeting antibodies (relative to all spike-targeting antibodies) did not vary with the interval between infection and the time of sample collection (Fig. S3). Therefore, the levels of antibodies elicited against the RBD and NTD are highly correlated and exhibit a relatively constant relationship in different infected individuals.

**Different domains, subunits, and oligomeric forms of spike show similar abilities to estimate the neutralization efficacy of COVID-19 convalescent-phase samples.**

Neutralizing antibodies mainly target the RBD and NTD of spike (9, 16, 17). Previous studies have shown that the levels of antibodies against different forms of spike (including S1, S1/S2,

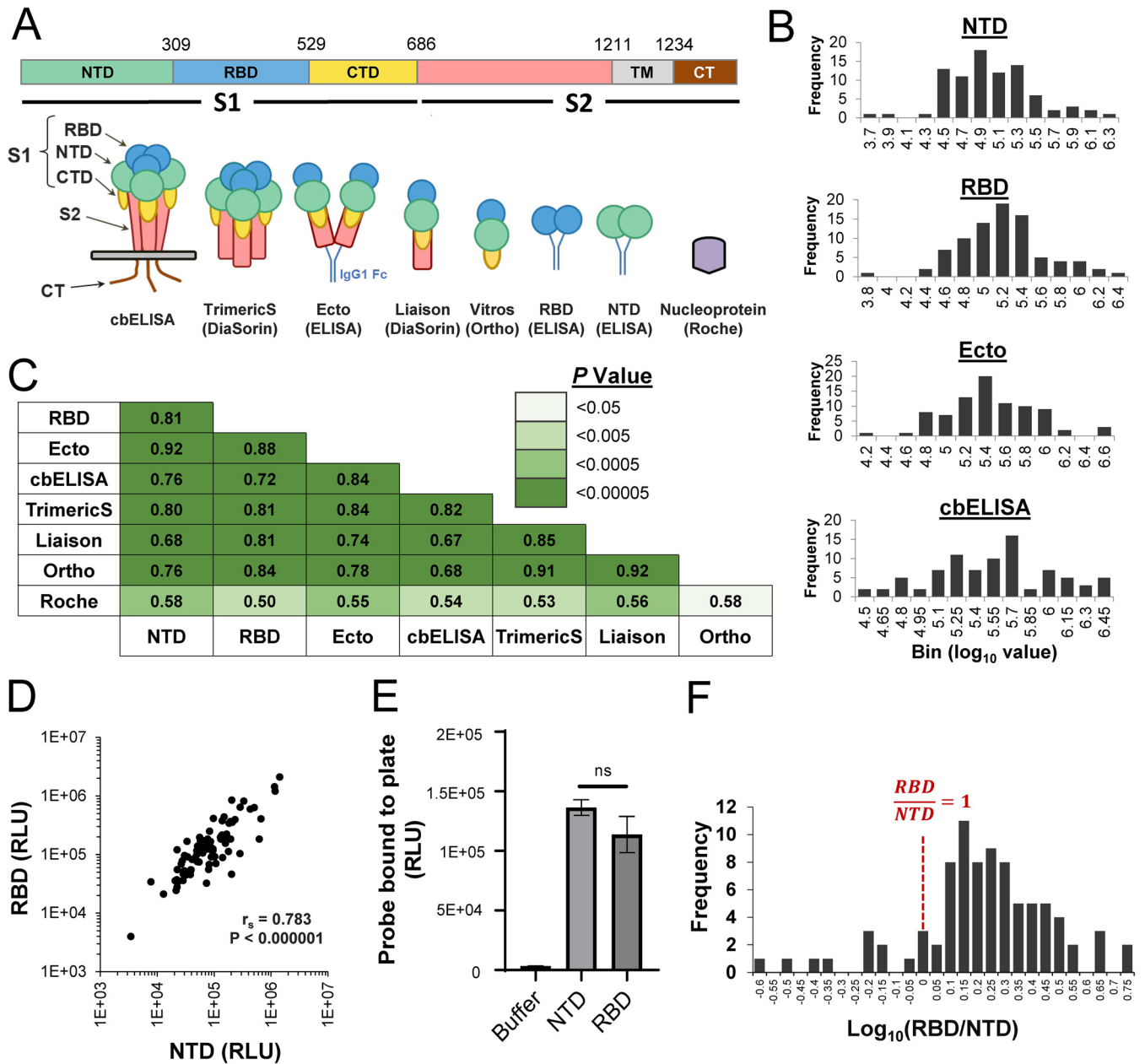


**FIG 1** Comparison of immunoassays that apply different components of the SARS-CoV-2 spike protein as capture antigens. (A) (Top) domains of the spike protein. NTD, N-terminal domain; RBD, receptor-binding domain; CTD, C-terminal domain; TM, transmembrane domain; CT, cytoplasmic tail. (Bottom) Schematic of the constructs used as capture antigens in this study. (B) SARS-CoV-2 antibody levels in 85 convalescent-phase serum and plasma samples were tested using the RBD, NTD, and Ecto ELISAs, as well as the cell-based ELISA. Distributions of the  $\log_{10}$ -transformed values are shown (see similar plots for commercial assays in Fig. S1C). (C) Spearman rank correlation coefficients between values measured in the eight immunoassays. Cells are colored by the  $P$  values determined in a two-tailed test. (D) Correlation between values in ELISAs that apply the NTD and RBD as capture antigens. RLU, relative light units.  $r_s$ , Spearman correlation coefficient;  $P$  value, two-tailed test. (E) Binding of the NTD and RBD probes to the ELISA plates. Equimolar concentrations of the NTD and RBD probes (25 nM) were incubated in 96-well protein-binding plates. Some wells were incubated with buffer alone. A secondary horseradish peroxidase-conjugated antibody was then added to the wells and its binding quantified by luminescence. ns, not significant. (F) Distribution among the 85 convalescent-phase samples of the ratio between log-transformed values measured in the RBD and NTD assays.

and RBD) correlate well with the neutralization capacity of the samples (27–32). However, the relationship between the neutralizing activity of the polyclonal response in each individual and its domain specificity, as well as the variation in this relationship between different hosts, is still poorly characterized. To address these questions, we compared the neutralization efficacy of the convalescent-phase samples and their binding to the capture antigens that represent different domains and forms of spike. To quantify neutralization, we first used a replication-defective pseudovirus that contains the spike protein of SARS-CoV-2. For this purpose,

we generated vesicular stomatitis virus (VSV) pseudovirions that encode the firefly luciferase gene in place of the native VSV-G glycoprotein gene and are pseudotyped with SARS-CoV-2 spike (VSV-SARS2-S) (5, 33). Residual infectivity of the pseudovirus in the presence of sera was measured using Vero-E6 target cells. The calculated dilution of serum at which virus infectivity was reduced 2-fold is reported as the  $IC_{50}$ . The  $\log_{10}$ -transformed  $IC_{50}$ s were consistent with a normal distribution ( $P = 0.329$  in a Shapiro-Wilk test), with a median  $IC_{50}$  corresponding to a dilution of 1:914 (Fig. 2A). For each sample, immunoassay values from each of the 7 different spike immunoassays were compared with the measured  $IC_{50}$ s (Fig. 2B). As expected, strong correlations were observed for all spike-based assays, as determined by the Spearman rank correlation coefficient, with  $P$  values lower than 0.000002 for all assays other than the nucleocapsid-based Roche test (Fig. 2C). These findings correspond with previous studies, which showed that spike-based immunoassays exhibit better correlations with  $IC_{50}$ s than the nucleocapsid-based Roche assay (34–36).

While there is a clear relationship between immunoassay values and neutralization efficacies in all comparisons, our primary question concerned the relative balance of these two factors in each assay, requiring a different metric. To better assess the relative abilities of the different capture antigens to estimate neutralization efficacies of the donor samples we used the precision metric. Precision was calculated by the ratio between the number of samples that are positive for neutralization (at the selected threshold) and the number of samples that are positive for SARS-CoV-2 antibodies by their immunoassay values. The level of precision was determined for subsets of the samples with progressively higher immunoassay thresholds for inclusion; from the 0th percentile (all samples are included in the test) to the 98th percentile (only samples with the top 2% of immunoassay values are included). Specific thresholds for neutralization were tested first, whereby a sample was considered neutralization positive if the  $IC_{50}$  was greater than a dilution of 1:500 or 1:2,000 (Fig. 3A). As expected, the use of samples from higher immunoassay percentiles resulted in higher precision. Differences between the immunoassays were more pronounced when the high neutralization threshold (1:2,000) was set. At this threshold, precision of the nucleocapsid-based Roche assay was low. Surprisingly, the cbELISA, which measures binding of antibodies to the native membrane-associated form of spike, also exhibited lower precision than other spike-based assays.

Given that performance of the assays can vary between neutralization thresholds, we sought to generate a metric that would describe performance across a range of thresholds. To this end, we first calculated for each threshold (from 1:500 to 1:2,500) the minimal immunoassay percentile required to achieve a precision level of 0.9 (see the boundary line for Ecto ELISA as an example in Fig. 3B and all assays in Fig. S4). The area above the boundary line, highlighted in green in Fig. 3B, indicates the percentile-threshold combinations that yield a precision of 0.9 or higher, which allows us to compare overall performance characteristics between immunoassays; the greater the area, the higher the ability of the assay to predict neutralization across all  $IC_{50}$  thresholds. The highest performance was observed for the Ortho, Liaison, Ecto, and RBD assays, followed by NTD, TrimericS, and cbELISA (Fig. 3C). Since the Roche assay did not achieve a precision of 0.9, the areas above the curve could not be computed. We then calculated the area above the curve when the required precision was set at levels ranging between 0.75 and 0.95. For most precision requirement levels in this range, the lowest performance was observed for the Roche assay, followed by cbELISA, with modestly better performance for the TrimericS and NTD (Fig. 3D). All other assays exhibited similar performance across the different precision requirements.

To determine statistical significance of the differences between performance of any two assays, we performed a permutation-based test. Briefly, for each pair of assays compared, we measured the area above the curve and calculated the difference between these values. We then permuted for each patient sample the immunoassay identifiers, recalculated the area above the curve for both immunoassays, and determined the difference. The fraction of the times the difference was greater using the

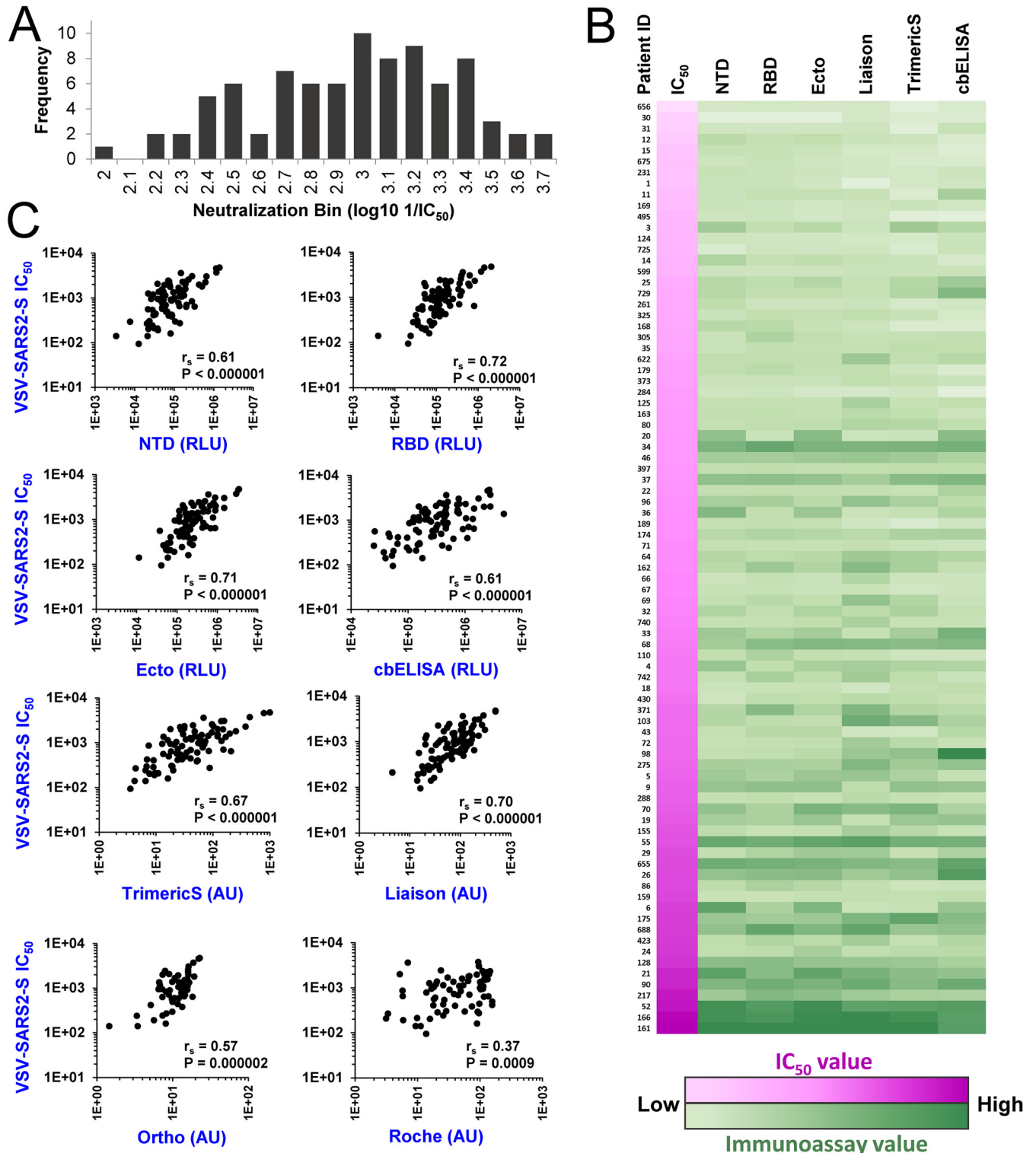


**FIG 2** Relationships between immunoassay values of COVID-19 convalescent-phase samples and their neutralization of spike-containing pseudovirus. (A) Neutralization titers of the serum or plasma samples were measured using replication-defective pseudovirus that contains the spike protein of SARS-CoV-2. Data describe the distribution of the  $\log_{10}$ -transformed  $IC_{50}$ s. (B) Comparison of neutralization and immunoassay values. All 85 samples are ordered by their neutralization titers (color coded in shades of pink, with low values in lighter shades). Values measured in immunoassays are color coded in shades of green. (C) Correlations between immunoassay values and neutralization titers.  $r_s$ , Spearman correlation coefficient.  $P$  values were determined with a two-tailed test.

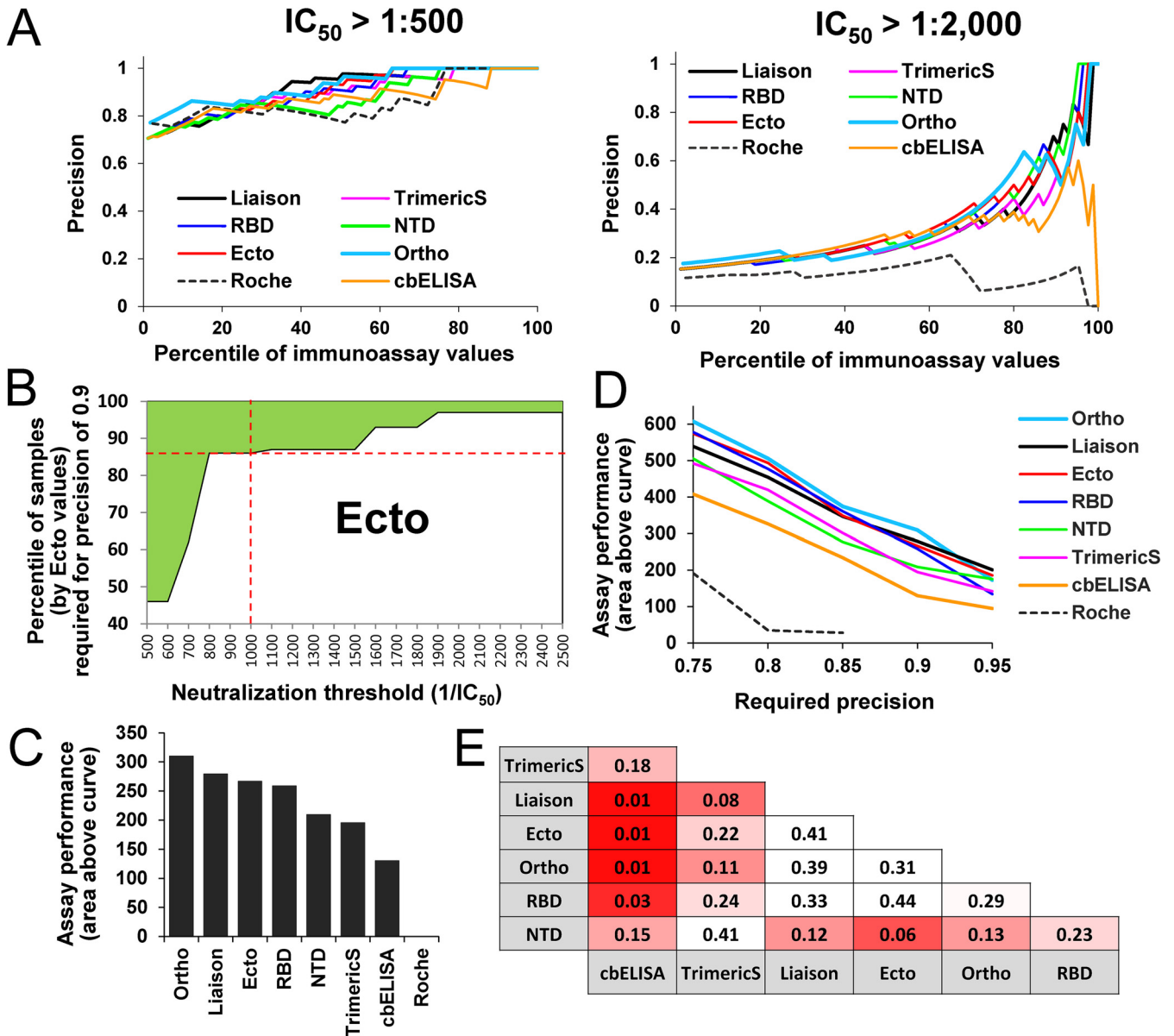


**FIG 3** Precision of immunoassays to estimate the neutralization efficacy of COVID-19 convalescent-phase serum and plasma. (A) Calculations of precision across different immunoassay percentiles. Precision was calculated as the number of samples with an  $IC_{50}$  greater than the defined threshold relative to the number of samples in the immunoassay percentile tested. Each data point describes precision of an immunoassay to predict neutralization at the indicated  $IC_{50}$  threshold using the indicated percentile of samples. (B) Area above the curve metric. The border between the shaded and unshaded areas describes the percentiles of Ecto values required to predict neutralization at the indicated thresholds with a precision of 0.9. For example, the intersection between the red lines indicates that, to predict with a precision of 0.9 for a threshold  $IC_{50}$  of 1:1,000, samples with Ecto values in the 85<sup>th</sup> percentile should be used. The shaded area describes all neutralization threshold-percentile combinations that yield a precision of 0.9 or higher. (C) Area above the curve shown in panel B calculated for all immunoassays, based on a required precision of 0.9. (D) Calculations of the area above the curve for required precision levels of 0.75 to 0.95. (E) Statistical significance of the differences between predictive capacity of the immunoassays. The area above the curve was calculated for all immunoassays for a precision of 0.9. Significance of the difference between predictive capacity of any two assays was determined by a permutation test. *P* values of a one-sided test are shown. Cells are color coded by the *P* values calculated.

permuted values than with the nonpermuted values was calculated as the *P* value. Significant differences for a one-sided test (*P* values lower than 0.05) were observed between the cbELISA and all other spike-based assays. The NTD and TrimericS assays showed moderate differences from other assays; however, they were not significant at the 95% confidence level (Fig. 3E). Therefore, the ability of cbELISA (i.e., the full-length membrane-bound form of spike) to predict neutralization was significantly lower than that of all other assays that apply isolated domains of the protein as capture antigens.

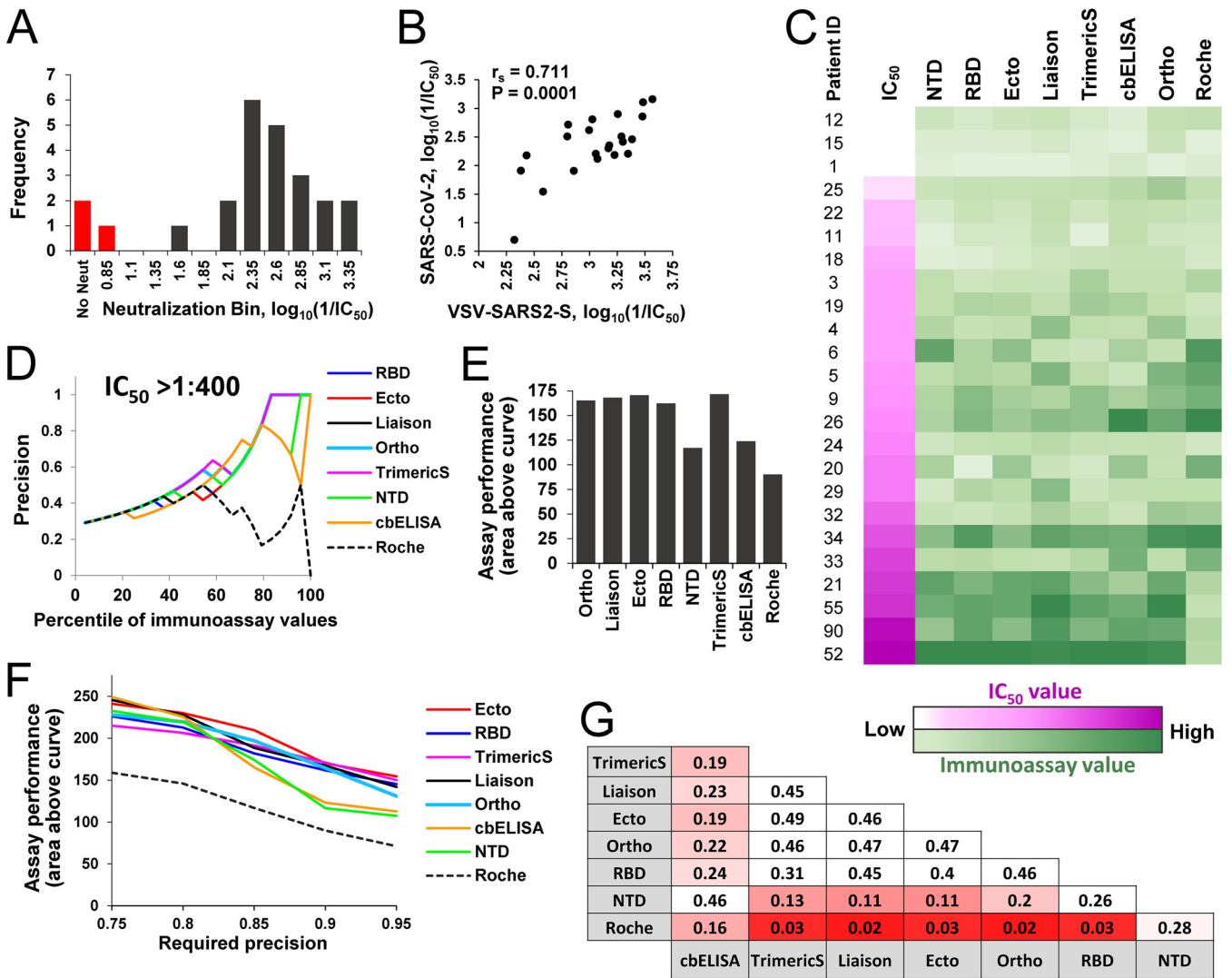


**FIG 4** Immunoassay-based estimations of replicative SARS-CoV-2 neutralization. (A) Twenty-four serum samples were tested for their neutralization of replicative SARS-CoV-2. The distribution of  $IC_{50}$ s is shown. For three samples, the  $IC_{50}$  was not achieved at the lowest dilution (1:40) of the serum (bars colored in red). (B) Correlation between  $IC_{50}$ s of the 24 serum samples, as measured using replication-competent SARS-CoV-2 and the VSV-SARS2-S pseudovirus. (C) Comparison of neutralization and immunoassay values. Samples are ordered by their efficacy of neutralization of replicative SARS-CoV-2 (color coded in shades of pink, with low values in lighter shades). Values measured in immunoassays are color coded in shades of green. (D) Precision of immunoassays to estimate SARS-CoV-2 neutralization at an  $IC_{50}$  threshold of 1:400 using different percentiles of the samples based on their immunoassay values. (E) Area above the curve calculated for a required precision of 0.9. (F) Performance of immunoassays to estimate neutralization at precision levels of 0.75 to 0.95. (G) Statistical significance of the differences between predictive capacities of the immunoassays, as determined by a permutation test. Calculations apply the area above the curve computed for a required precision of 0.9.  $P$  values of the one-sided test are shown. Cells are color coded by the  $P$  values.

To independently validate the above findings, we also measured neutralization titers for 24 of the serum samples using infectious SARS-CoV-2 under BSL-3 conditions and correlated those findings with immunoassays values. Virus-induced cytopathology was used to detect infection. The dilution of serum at which cytopathic effects were observed in fewer than 50% of the wells was determined, and data were fitted to a regression model to calculate the precise  $IC_{50}$ . For three of the samples, the  $IC_{50}$  was not achieved at the lowest dilution of the serum used (1:40); the remainder showed a range of  $IC_{50}$ s, with a median dilution of 1:212 (Fig. 4A). A strong correlation was observed between the neutralization titers of the sera measured using the replicative SARS-CoV-2 and the VSV-based pseudovirus that contains the spike protein (Fig. 4B). As expected,  $IC_{50}$ s in the pseudovirus assay were higher than those measured using infectious virus, since the former measures the dilution at which 50% of virus infectivity is reduced, whereas the latter measures the dilution at which more than 50% of wells show complete neutralization of all input virus.

We compared immunoassay values of the samples with their neutralization efficacies of replicative SARS-CoV-2 (Fig. 4C). Strong correlations were observed for all spike-based assays (Fig. 55). Precision analyses using an  $IC_{50}$  threshold of 1:400 demonstrated considerable differences between performance of the assays (Fig. 4D). Comparison of the overall performance of the immunoassays across neutralization thresholds of 1:50 to 1:500 (using the area above the curve metric with a required precision of 0.9) showed a similar pattern to the pseudovirus-based measurements (compare Fig. 4E and Fig. 3C); the poorest performance was observed for the Roche assay, followed by NTD and cbELISA. All other assays performed similarly well. Comparison of assay performance at precision levels of 0.75 to 0.95 showed modest differences between cbELISA or NTD and all other spike-based assays (Fig. 4F); however, these differences did not reach a significance level of 0.05 (Fig. 4G).

Therefore, comparison of the precision of immunoassays to predict neutralization using pseudoviruses containing SARS-CoV-2 spike or replication-competent virus yielded roughly similar findings. The performance of assays based on RBD, S1, or monomeric and dimeric forms of S1/S2 was comparable, with the highest precision observed for Ortho, Ecto, and Liaison. Modestly lower performance was observed for the soluble trimeric form of spike (TrimericS) and still lower performance for the NTD and full-length spike measured by cbELISA.

**COVID-19 convalescent-phase samples exhibit similar levels of relative neutralization potency.** The relationship between the levels of NTD and RBD antibodies is relatively conserved in different individuals (Fig. 1D). Antibodies that target these domains can neutralize SARS-CoV-2 infection (10, 11, 26, 37, 38). We asked whether neutralization efficacy increases with higher proportions of RBD- or NTD-targeting antibodies (relative to all spike-targeting antibodies). Comparison of the RBD-to-Ecto or NTD-to-Ecto ratios with the neutralization efficacy of the samples showed no evidence for a relationship between these variables (Fig. 5A and B). Similarly, the RBD-to-NTD ratio was not associated with the neutralization efficiency of the samples (Fig. 5C). These findings indicate that convalescent-phase samples with high neutralizing activity do not contain a higher proportion of antibodies that target the RBD or NTD.

A large proportion of spike-targeting antibodies elicited by infection are nonneutralizing (39, 40). A recent study showed that infected and immunized hosts with high levels of spike-specific antibodies generate a significantly higher proportion of nonneutralizing antibodies than individuals with lower levels of anti-spike antibodies (37). To explore this relationship in our samples, we implemented a model to examine evidence for a variable ratio between immunoassay values and neutralization efficacy. Two computational approaches were used; the first looks for nonlog linearity in the relationship between neutralization and immunoassay tests, whereas the second considers their rank ratios and examines evidence for a systematic change over the ranks of the immunoassay results.

To compare the variables and avoid a bias related to the dynamic ranges of the values, we corrected the  $\log_{10}$ -transformed immunoassay and neutralization  $IC_{50}$ s to the same scale by adjustment to a range from 0.1 to 1. For each sample we calculated the ratio between the immunoassay value and the  $IC_{50}$  (see analysis of the Ecto ELISA data in Fig. 5D). This ratio was compared between the 20 samples with the lowest immunoassay values and the 20 samples with the highest immunoassay values. Evaluation of these results did not find significantly different ratios in the two groups (see *P* values for an unpaired *t* test in Fig. 5D). A similar lack of a significant difference was observed when the RBD and NTD were used as capture antigens (Fig. 56). However, the cbELISA results suggested a higher ratio (i.e., a lower relative neutralization efficacy) for the samples with high antibody levels. This finding may result from detection of different subsets of antibodies by the full-length form of spike used in the cbELISA relative to the soluble forms applied as probes in the other assays.

To further explore whether the immunoassay-to-neutralization ratio shows any indication of dependence on the immunoassay value, we examined the variability in this ratio by looking for nonlinearity in their log-relationship using all 85 samples. The null

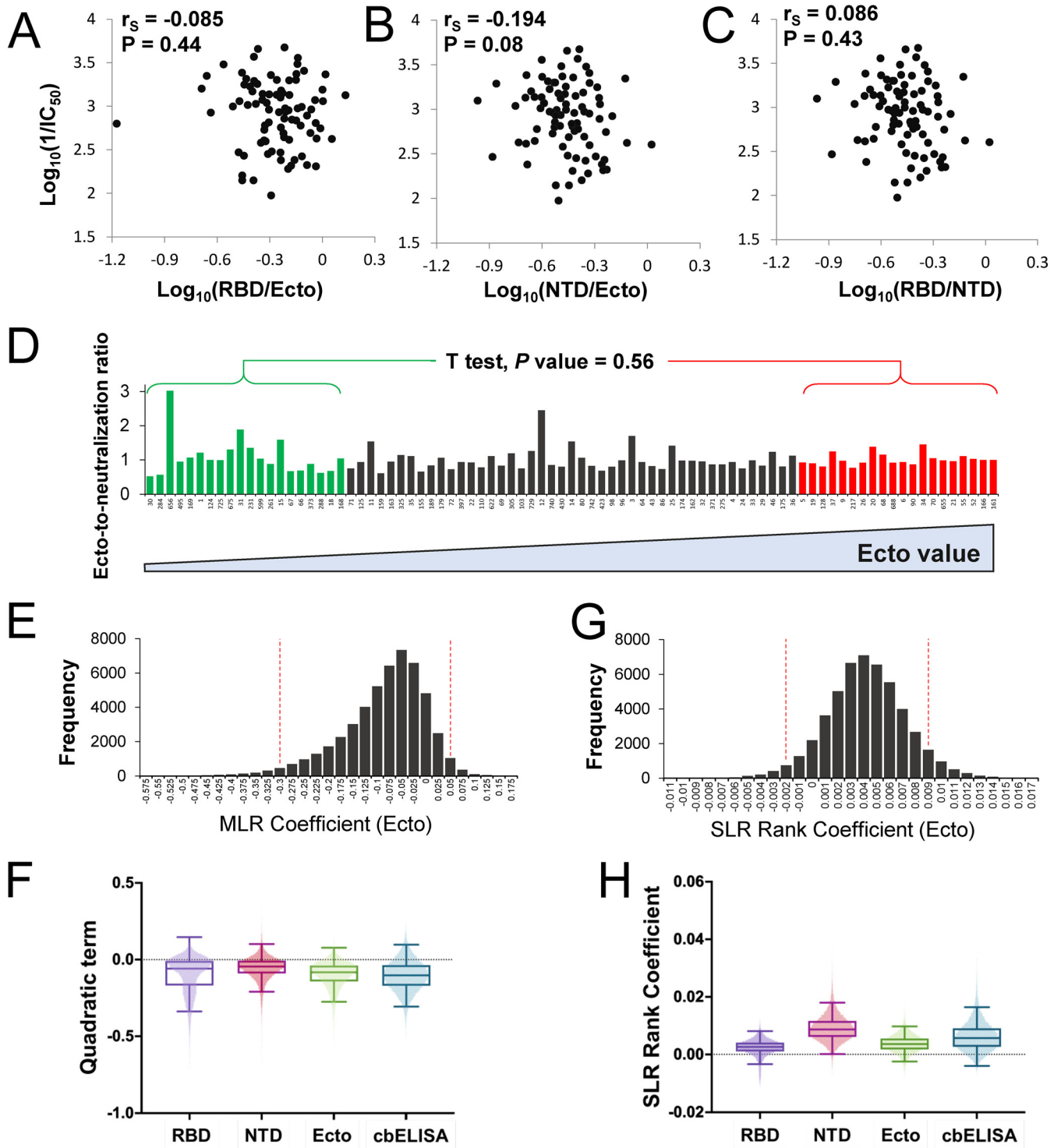


**FIG 5** Relationship between the relative neutralizing potency of convalescent-phase samples and their content of spike-specific antibodies. (A and B) Comparison of the relative RBD or NTD binding values (expressed as a fraction of the Ecto value) and neutralization efficacy of the samples. (C) Comparison of the ratio between RBD and NTD values and neutralization efficacy. (D)  $IC_{50}$ s of convalescent-phase samples and their immunoassay values were  $\log_{10}$  transformed and adjusted to a scale of 0.1 to 1. The ratio between the Ecto ELISA value and the  $IC_{50}$  of each sample was calculated for all samples. Patient samples are arranged by increasing Ecto values, from left to right. The ratios calculated for the 20 samples with the lowest and the 20 samples with the highest Ecto values were compared using an unpaired  $t$  test; the  $P$  value for a two-tailed test is indicated. (E) Bootstrap distribution for quadratic term in MLR describing the relationship between log Ecto values and log  $IC_{50}$ s, evaluating evidence for a nonconstant ratio relationship. A 95% bootstrap confidence interval was determined from bootstrap sample quantiles. (F) The quadratic term was calculated by 50,000 iterations of bootstrap resampling for NTD, RBD, Ecto, and cbELISA data. The boxed area shows the second and third quartiles. Whiskers describe the range for two standard deviations. (G) Bootstrapped rank regression. The rank order of Ecto values for all 85 samples was determined as well as the ratio between the ranks of the

(Continued on next page)

hypothesis tested was that the log-scale relationship between these variables should be linear, which was tested by considering a quadratic term for immunoassay results in a multiple linear regression (MLR) model. While the data appeared well modeled directly on a  $\log_{10}$  scale, to eliminate concerns about distributional assumptions, the regression coefficient was bootstrapped and the corresponding 95% confidence interval determined. We first analyzed the results of the Ecto assay. As shown in Fig. 5E, an MLR slope value of 0 (i.e., lack of a quadratic effect, leaving a linear increase in neutralization activity for a given increase in binding) lies within the 95% confidence interval; therefore, we fail to reject the null hypothesis that the variables follow a ratio relationship. Similar analyses of the data from the NTD, RBD, and cbELISA tests also failed to show evidence at the 95% level to support a nonlinear relationship between immunoassay values and neutralization (Fig. 5F).

We also applied a rank-based approach, whereby immunoassay and neutralization values were transformed to their ranks (from 1 to 85). A simple linear regression (SLR) coefficient was then fitted to the relationship between the immunoassay rank value and immunoassay-to-neutralization rank ratio, and bootstrapping was applied to produce 95% confidence intervals. The null hypothesis tested was that a slope of 0 exists for this relationship. Again, no evidence was observed to support the notion that the ratio between Ecto values and neutralization varies across different levels of Ecto-targeting antibodies (Fig. 5G). A similar bootstrapping analysis of the rank values for the RBD, NTD, and cbELISA failed to demonstrate a nonzero slope that would indicate a linear relationship between the two variables (Fig. 5H).

Given the sample size ( $n = 85$ ), the presence of a strong relationship between neutralization fraction and antibody binding activity seems unlikely. Nevertheless, we did observe negative nonsignificant coefficients for the quadratic effect of log-binding activity on neutralization levels and positive nonsignificant coefficients of for the linear relationship between binding activity and the rank ratio of binding to neutralization (Fig. 5G and H). Both of these results indicate the plausibility of a weak relationship between the neutralization ratio and binding activity measures, in which higher binding activity could be associated with lower proportional neutralization activity, but the magnitude of such an effect is likely to be limited, decreasing the biological relevance of such effects.

## DISCUSSION

Over the course of the COVID-19 pandemic, our understanding of the antibody response against SARS-CoV-2 has evolved considerably. Initial investigations suggested that most neutralizing antibodies elicited by infection or vaccination target the RBD (9, 41). More recent studies have shown a codominance of antibodies that target the RBD and NTD (25, 26). Proteomic deconvolution studies of the IgG repertoire in COVID-19 convalescent patients suggested that the bulk of the neutralizing response targets epitopes outside the RBD (38). To better understand the target specificity of the response in different individuals, we analyzed the relative level of antibodies against different domains, subunits, and oligomeric forms of spike in COVID-19 convalescent-phase samples. Our findings suggest the model shown in Fig. 6. A polyclonal antibody response is elicited in each infected individual against multiple domains of spike. High variation is observed between individuals in the amounts of antibodies generated; however, there is limited variation in the relationship between the amounts of antibodies that target the RBD and NTD, with a ratio ranging between 1 and 3 in 78% of subjects. Importantly, the relative potency of the response (i.e., the level of neutralizing activity relative to the level of antibodies generated) is also constant in different individuals. Thus, the domain specificity and relative inhibitory activity of the response

### FIG 5 Legend (Continued)

Ecto value and  $IC_{50}$ . A simple linear regression model was fitted to the relationship between the two variables. A bootstrapping procedure was performed to estimate the slope coefficient. The bootstrap distribution and corresponding 95% confidence interval are shown. (H) The rank regression coefficient was calculated by bootstrap resampling using NTD, RBD, Ecto, or cbELISA data.

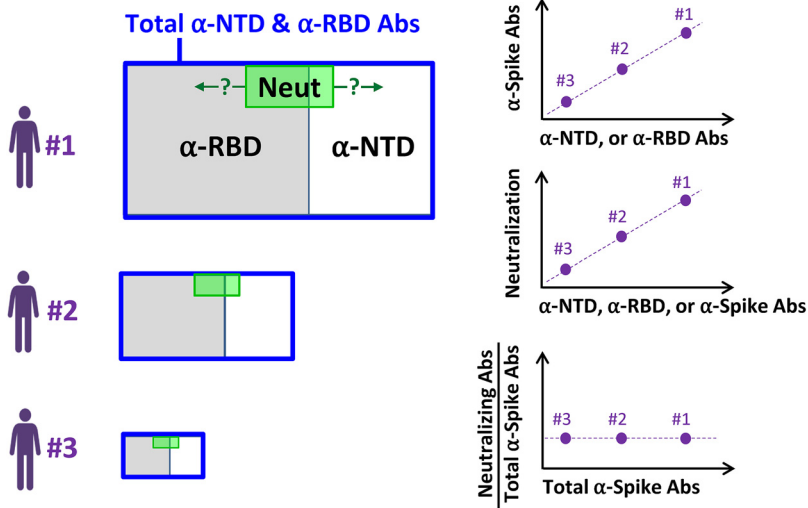


**FIG 6** Model of the polyclonal antibody response elicited against the SARS-CoV-2 spike protein. SARS-CoV-2-infected individuals generate different amounts of antibodies against the NTD and RBD of spike (represented by the size of the blue rectangles). The relationship between the amounts of antibodies that target the RBD and those against the NTD is constant in different individuals, with a mean RBD-to-NTD ratio of 1.8. The relative neutralization potency (represented by the green-shaded area) is also similar in different individuals. Question marks indicate the yet-unknown domain distribution of the fraction of antibodies that contains neutralizing activity (i.e., positioning of the green-shaded area).

are conserved among individuals, with the main variation being the total amount of the antibodies produced. We note that our samples were collected from individuals infected with SARS-CoV-2 at early time points of the COVID-19 pandemic (March 2020 to January 2021); as such, they document properties of the antibody responses to spike proteins that more closely resemble those of the SARS-CoV-2 ancestor. Since then, multiple mutations in the RBD and NTD have appeared in emerging variants of the virus, which alter its sensitivity to vaccine-elicited antibodies and likely its immunogenic properties (42–44). Whether these mutations have also changed the domain specificity patterns of the antibody responses and their relative neutralization potencies, as described here, remains to be determined.

Multiple commercial immunoassays have been developed that apply different components of the spike protein as the capture antigen (36, 45–48). Spike-based assays have been shown to estimate well the neutralization efficacy of convalescent-phase serum and plasma samples (27–30). They are thus applied as qualitative measures of immunization status and can potentially serve as indirect measures of the efficacy of the anti-SARS-CoV-2 humoral response. Our studies suggest that any soluble form of spike that contains the RBD or NTD can serve as a capture antigen to accurately determine the immunization status of the individual and potentially the efficacy of the anti-SARS-CoV-2 humoral response. The constant proportion of antibodies against different spike domains also explains the ability of immunoassays that use various forms of the protein as capture antigens to predict neutralization. Indeed, our findings suggest that determinations of neutralizing titers based on serological tests do not require native forms of the protein as the capture antigen; RBD exhibits a predictive capacity similar to that of S1 or the entire ectodomain, with only modestly lower performance for NTD. Thus, inclusion of S2 or trimerization of the protein to mimic the native form of spike does not improve the ability to estimate the amount of neutralizing antibodies. In fact, the poorest performance was observed for the full-length, membrane-bound form of the protein measured by cbELISA.

Several reasons may underlie the lower performance of the cbELISA relative to the assays that apply soluble forms of spike. First, the cleavage status of spike produced in HOS cells (used for the cbELISA) and 293T cells (used for producing virus and the

soluble probes) is likely different. Previous studies have shown that the envelope glycoproteins (Envs) of HIV-1 expressed on HOS cells are mostly in furin-cleaved form, whereas Envs on the surface of 293T cells are mostly uncleaved (49). Accordingly, we expect that most spike trimers expressed on the HOS cells are also cleaved, whereas spike produced in 293T cells is mostly uncleaved. Such differences may affect recognition of spike by some antibodies. Second, the glycosylation patterns of spike may differ between HOS cells and 293T cells. Different cell types exhibit diverse glycosylation patterns of viral proteins (50, 51). For example, the efficiency of binding of SARS-CoV-2 spike to the ACE2 receptor has been shown to differ between mammalian cells due to differences in glycosylation profiles of spike (52). Third, it is plausible that the full-length form of spike on the HOS cells may preferentially detect nonneutralizing antibodies. Indeed, the soluble probes do not contain spike regions in the C terminus of the S2 subunit, including the membrane-proximal external region (MPER) and cytoplasmic tail. Antibodies against S2, including the MPER, are frequently elicited in COVID-19 patients (40, 53). In addition, absence of the MPER and cytoplasmic tail may affect exposure of other S1 or S2 epitopes. Whereas cytoplasmic tail deletion does not appear to alter patterns of sensitivity to sera (54), this truncated form may exhibit a different profile of recognition by the nonneutralizing antibody fraction.

We were surprised to discover that subjects with different amounts of spike-specific antibodies contained a constant level of relative neutralization potency. Such results contrast with a recent study by Amanat et al., which suggested that convalescent-phase samples with large amounts of anti-spike antibodies (as measured by the Mount Sinai Laboratory COVID-19 ELISA IgG antibody test) contain a higher proportion of nonneutralizing antibodies against this protein (37). It should be noted that in their calculations, the authors analyzed the immunoassay-to-IC<sub>50</sub> ratios using the raw values obtained in these tests. Unfortunately, such an approach can introduce a bias if the dynamic ranges of the two variables differ. To address this potential bias, we performed our calculations using ranks and values that were corrected to the same scale. Both approaches showed similar results, whereby the relative potency is constant in different samples, regardless of the amount of anti-spike antibodies generated. Whether the target specificity of the neutralizing antibody fraction is also constant in different individuals and independent of the robustness of the response still remains to be determined. Such studies are of particular importance in vaccinated individuals, to accurately quantify and characterize specificity of the antibody fractions that can protect from infection.

## MATERIALS AND METHODS

**Collection of plasma and serum from donors and patients.** All blood donors were screened following the FDA guidance instructions under an institutional review board approved protocol (IRB number 202003554). The consent signed by all donors allowed the use of blood samples for research purposes. Donors were identified and screened following FDA guidelines at the time they enrolled. Two study groups were assessed. The first was composed of 57 convalescent-phase serum samples from subjects that had either been confirmed by reverse transcription-PCR (RT-PCR) to be SARS-CoV-2 positive from a nasopharyngeal swab ( $n = 51$ ) or had signs or symptoms of COVID-19 and were found to be positive by serological testing ( $n = 6$ ). All donors except one had relatively mild COVID-19 symptoms; this donor was hospitalized for 1 day due to palpitations. Donor screening was performed at least 10 days after resolution of symptoms. At the time of plasma collection, serum samples were collected in serum separator tubes and allowed to clot for at least 30 min. Serum was then isolated, aliquoted, and stored at  $-80^{\circ}\text{C}$  until use. The second study group was composed of convalescent-phase plasma samples collected from women hospitalized for delivery who had previously been infected by SARS-CoV-2, as confirmed by a SARS-CoV-2-positive PCR ( $n = 7$ ) or positive serology test ( $n = 21$ ). Samples were collected in EDTA-containing tubes, aliquoted, and frozen until use at  $-80^{\circ}\text{C}$ .

**Cells lines.** Vero-E6 cells, human embryonic kidney (HEK) 293T cells, and human osteosarcoma (HOS) cells were obtained from the American Type Culture Collection (ATCC). Cells were cultured in Dulbecco's modified Eagle medium (DMEM) supplemented with 2 to 10% fetal calf serum (FCS) and 1% penicillin-streptomycin. All cells were maintained in a humidified incubator at  $37^{\circ}\text{C}$  and 5%  $\text{CO}_2$ .

**Recombinant proteins and their production.** Capture antigens that contain different spike protein components were generated. The NTD, RBD, or ectodomain of S1/S2 (Ecto) antigens were fused to the Fc region of human IgG1, rendering them dimeric. NTD and RBD contain amino acids 1 to 309 and 310 to 529 of spike, respectively. The Ecto protein contains the entire ectodomain of spike (amino acids 1 to

1211). To abrogate the furin cleavage site in Ecto, we replaced the Arg-Arg-Ala-Arg motif at position 683 to 686 with Ser-Ser-Ala-Ser. All proteins were produced by transient transfection of 293T cells using polyethyleneimine (PEI), as previously described (55). Proteins were harvested in 2935 ProCDM and purified using protein A beads. Eluted products were dialyzed against phosphate-buffered saline (pH 7.4). All proteins were analyzed by SDS-PAGE and visualized by silver staining to verify their molecular weight and purity.

**ELISA using RBD, NTD, and Ecto as capture antigens.** The RBD, NTD, and Ecto recombinant proteins were used as capture antigens in an enzyme-linked immunosorbent assay (ELISA). Briefly, proteins were suspended in PBS at a concentration of 25 nM (2  $\mu\text{g}/\text{ml}$  of NTD, 1.37  $\mu\text{g}/\text{ml}$  of RBD, and 5  $\mu\text{g}/\text{ml}$  of Ecto) and incubated overnight in protein-binding 96-well plates (PerkinElmer). The next day, wells were washed once with blocking buffer, composed of 140 mM NaCl, 1.8 mM  $\text{CaCl}_2$ , 1 mM  $\text{MgCl}_2$ , 25 mM Tris (pH 7.5), 20 mg/ml bovine serum albumin (BSA), and 1.1% nonfat dry milk. Serum or plasma samples were diluted 1:500 (vol/vol) in blocking buffer, added to the wells, and incubated for 45 min at room temperature. Samples were then washed four times with blocking buffer, and a horseradish peroxidase (HRP)-conjugated secondary antibody that targets the kappa light chain of human IgG1 was added (diluted 1:1,200 in blocking buffer). After incubation for 1 h at room temperature, samples were washed 5 times with blocking buffer and 5 times with washing buffer (140 mM NaCl, 1.8 mM  $\text{CaCl}_2$ , 1 mM  $\text{MgCl}_2$ , and 25 mM Tris [pH 7.5]). HRP enzyme activity was measured by light emission using SuperSignal West Pico Plus chemiluminescence detection reagents with a Synergy H1 microplate reader.

**Cell-based ELISA measurements of antibodies against SARS-CoV-2 spike.** Binding of serum antibodies to SARS-CoV-2 spike expressed on HOS cells was measured using a previously described cell-based ELISA system (22, 24). Briefly, HOS cells were seeded in white opaque 96-well plates ( $1.4 \times 10^4$  cells per well) and transfected the next day with 80 ng per well of pCG1-SARS-2-S plasmid expressing SARS-CoV-2 spike using JetPrime transfection reagent. To quantify background binding of the antibodies to the cells, a similar number of wells was transfected using a negative-control plasmid ( $\Delta\text{KS}$ ) that does not encode a viral protein product (23). Three days after transfection, cells were washed with blocking buffer, and serum samples diluted 1,000-fold in blocking buffer were incubated with the cells for 1 h at room temperature. Cells were then washed 5 times with blocking buffer and incubated for 45 min at room temperature with an HRP-conjugated goat anti-human kappa chain preparation that was diluted 1:1,200 in blocking buffer. Cells were then washed 5 times with blocking buffer and 5 times with washing buffer. HRP enzyme activity was measured by chemiluminescence with a Synergy H1 microplate reader.

**Commercial immunoassays to measure antibodies that target SARS-CoV-2 proteins.** The DiaSorin Liaison SARS-CoV-2 S1/S2 IgG chemiluminescence assay detects IgG against spike subunits S1 and S2. Samples were analyzed according to the manufacturer's guidelines on a DiaSorin Liaison XL automated chemiluminescence analyzer (DiaSorin, Saluggia, Italy). A signal of 15 arbitrary units (AU) per ml or higher is defined by the manufacturer as a positive result. The DiaSorin TrimericS IgG assay applies the soluble trimeric form of the S1/S2 subunits. Samples were analyzed on a DiaSorin Liaison XL automated chemiluminescence analyzer. A signal of 13 AU/ml is defined as a positive result. The Roche electrochemiluminescence immunoassay measures total immunoglobulins against SARS-CoV-2 nucleocapsid (N) protein. Samples were analyzed according to the manufacturer's guidelines using the Elecsys Anti-SARS-CoV-2 assay on the Roche cobas e602 platform (Roche Diagnostics). A cutoff index (COI) of 1.0 or higher is defined by the manufacturer as a positive result. The Ortho COVID-19 IgG antibody test was performed on Ortho's VITROS system. The signal-at-cutoff (S/C) value as defined by the manufacturer is 1 unit or greater for a reactive sample. For simplicity, all values of the commercial assays are reported in arbitrary units.

**Infection and neutralization of replication-competent SARS-CoV-2.** SARS-CoV-2 strain USA-WA1\_2020 was obtained from BEI Resources and maintained under biosafety level 3 (BSL-3) conditions. To propagate virus, Vero-E6 cells cultured in DMEM–2% FCS were infected at a multiplicity of infection (MOI) of 0.001. Forty-eight hours after infection, supernatants were harvested, filtered through 0.45- $\mu\text{m}$ -pore-size membranes, and frozen at  $-80^\circ\text{C}$  until use. To quantify the amount of infectious virus, Vero-E6 cells were seeded in 96-well plates ( $1.5 \times 10^4$  cells per well). The next day, serial dilutions of the virus were added to 8 replicate wells for each dilution and cytopathic effects were evaluated over the next 5 days. The median tissue culture infectious dose ( $\text{TCID}_{50}$ ) was used to quantify virus titer, which describes the dilution of the virus at which fewer than half of the replicate wells show cytopathic effects.

To measure neutralization, serial 2-fold dilutions of the serum samples (ranging from 1:40 to 1:2,560) were prepared in DMEM–2% FCS. Virus was added to the diluted serum at a final concentration of 25  $\text{TCID}_{50}$  per well. Samples were incubated at room temperature for 1 h and added to Vero-E6 cells seeded the day before in 96-well plates ( $1.5 \times 10^4$  cells per well). Six replicate wells were used for each dilution. Cells were then cultured for 4 days at  $37^\circ\text{C}$  until infectivity was evaluated. The number of wells in which intact monolayers were present was assessed using an inverted light microscope. The 50% neutralizing titer ( $\text{IC}_{50}$ ) was calculated by the serum dilution at which 50% or more of the wells showed no cytopathic effects. To determine the precise  $\text{IC}_{50}$ , the number of wells in which cytopathic effects were observed at each serum dilution was recorded. These values, along with the log-transformed dilution values were fitted to a nonlinear regression model using GraphPad Prism 8 to calculate the  $\text{IC}_{50}$ .

**Production and neutralization of vesicular stomatitis virus pseudotyped by the SARS-CoV-2 spike protein.** Vesicular stomatitis virus (VSV) pseudovirions bearing the SARS-CoV-2 spike protein (VSV–SARS2-S) were generated as previously described (5). Briefly, 293T cells were seeded in 100-mm plates ( $2.2 \times 10^6$  cells per plate) and transfected 24 h later by 16  $\mu\text{g}$  of pCG1-SARS-2-S plasmid (a kind gift from Stefan Pöhlmann) using a PEI transfection protocol (55). Twenty-four hours after transfection, cells were infected with a stock of VSV pseudovirus that contains the firefly luciferase gene in place of the native VSV-G glycoprotein gene and encodes the glycoprotein of Lassa virus (5). Six hours later, infected cultures were washed twice with phosphate-buffered saline (PBS, pH 7.4) to remove input

pseudovirions, and fresh DMEM–2% FCS was added. Medium was collected at 24 and 48 h after infection, the supernatants were filtered through 0.45  $\mu\text{m}$  pore-sized membranes and centrifuged at  $5,380 \times g$  for 16 h at 4°C. The pellet was resuspended in PBS and centrifuged through a 20% sucrose cushion at  $134,000 \times g$  for 2 h at 10°C. Pellets containing the pseudoviruses were resuspended in PBS and stored at  $-80^\circ\text{C}$  until use.

For neutralization assays, 2-fold serial dilutions of the serum samples were prepared in DMEM–5% FCS, ranging between 1:40 and 1:2,560. Viruses were added to the diluted serum at a concentration calculated to yield between 100,000 and 200,000 relative light units (RLUs) of luciferase activity per well. These values were determined to be within the linear range of virus input versus luciferase activity measured. Vero-E6 target cells were seeded the day before infection in 96-well white opaque flat-bottomed plates ( $1.5 \times 10^4$  cells per well). The virus-serum or virus-plasma mixture was incubated for 1 h at 37°C and added to the wells. Six replicate wells were used for each condition. Samples were then incubated for 24 h at 37°C, after which the media were removed and 35  $\mu\text{l}$  of passive lysis buffer (Promega) was added to each well. Luciferase activity was recorded as a measure of viral infection, as previously described (24). Briefly, 100  $\mu\text{l}$  of luciferin buffer containing 15 mM  $\text{MgSO}_4$ , 15 mM  $\text{KPO}_4$  (pH 7.8), 1 mM ATP, and 1 mM dithiothreitol was added to each well, followed by 50  $\mu\text{l}$  of 1 mM D-luciferin potassium salt (Syd Laboratories). Luminescence was detected using a Synergy H1 Hybrid reader (BioTek Instruments).

**Permutation test to compare precision of immunoassays.** For each immunoassay, we obtained the curve that describes the required percentile of samples for each neutralization threshold to yield a precision of 0.9. The area above the curve was then determined, which describes all percentile-neutralization threshold combinations that yield a precision level higher than the minimum precision of interest (here, 0.9). This metric thus captures the precision of each assay across multiple neutralization thresholds. To test for significant difference between the area above the curve for any two immunoassays, we used a permutation test. The null and alternative hypotheses for a one-sided test can be stated as follows:  $H_0: A_i = A_j$ ,  $H_1: A_i > A_j \neq j$  and  $i, j = 1, 2, \dots, M$ , where  $A_i$  and  $A_j$  describe the area above the curve for immunoassays  $i$  and  $j$ , respectively, and  $M$  is the total number of immunoassays tested. To test the above hypothesis, we first log-transformed immunoassay values and standardized them to a scale of 0 to 1:  $X_{new}^i = [X^i - \min(X^i)] / [\max(X^i) - \min(X^i)]$ , where  $X^i$  is the vector of values for immunoassay  $i$ . The difference between the area above the curve for  $i$  and  $j$  was then calculated, denoted as  $D_{ij}$ . We then performed a permutation test whereby we permuted for each patient sample the immunoassay identifiers and the area above the curve was recalculated for each immunoassay. This process was repeated 1,000 times ( $k = 1, 2, \dots, 1,000$ ). The difference between the areas above the curves for each iteration of the permutation test was defined as  $d_{ij}^k$ . The number of instances in which the permuted value of  $d_{ij}^k$  was greater than or equal to the nonpermuted  $D_{ij}$  was calculated and expressed as a fraction of the number of iterations performed, which was defined as the  $P$  value for testing the null hypothesis.

**Multiple linear regression and rank-based simple linear regression.** In the absence of a universal gold standard,  $\log_{10}$  transformations appeared reasonable to capture immunoassay values and neutralization activity. Under our null hypothesis, a change in binding activity,  $\log_{10}(X)$ , should be associated with a linear increase in neutralization,  $\log_{10}(Y)$ . This relationship can be expressed as a linear regression on the log-scale:  $\log(y) = \beta_0 + \beta_1 \log(x) + \epsilon$ . A simple way of detecting departures from this model is to look for curvature in the effect of  $\log(x)$ :  $\log(y) = \beta_0 + \beta_1 \log(x) + \beta_2 \log(x)^2 + \epsilon$ . Any evidence that  $\beta_2$  is nonzero will show departure from the hypothesized relationship; for example, if higher values of binding activity produce a diminished change in neutralization efficacy, we would expect  $\beta_2$  to be negative. We therefore fitted a multiple linear regression with the outcome variable of  $\log \text{IC}_{50}$  and each of the log-scale immunoassay variables in turn as  $X$ . To avoid any problematic assumptions about the distribution of the error term  $\epsilon$ , the MLR was fitted under a bootstrapping procedure, in which 50,000 repeated samples were taken to produce a bootstrap distribution of the parameter estimates. This was used to compute nonparametric 95% confidence intervals for the  $\beta_2$  quadratic effects.

In addition to this MLR approach using log-transformed assay values, we conducted a series of rank-based analyses. Rather than focusing on the ratio relationship directly, we hypothesized that high neutralization values (relative to the sampling distribution) should correspond to high binding values (relative to the sampling distribution), in such a way that the rank ratios,  $X_r/Y_r$ , should follow a distribution with mean not depending on the binding rank,  $X_r$ . This was investigated via a bootstrapped simple linear regression with the rank ratio of binding to neutralization as the outcome and the binding rank as the single explanatory variable. Under the null hypothesis, the slope parameter for the binding rank,  $\beta_1$ , should be equal to zero. We again performed 50,000 repeated samples to produce bootstrap distributions and corresponding nonparametric confidence intervals for  $\beta_1$ .

## SUPPLEMENTAL MATERIAL

Supplemental material is available online only.

**SUPPLEMENTAL FILE 1**, PDF file, 0.4 MB.

**SUPPLEMENTAL FILE 2**, XLSX file, 0.02 MB.

## ACKNOWLEDGMENTS

We thank all blood donors that contributed samples to this study and Julie Kurt from the Department of Pathology and Mary Rysavy and Kim Kenne from the Department of Gynecology and Obstetrics at the University of Iowa for assistance in coordinating these studies. We also thank Michelle Sexton of the Iowa State Hygienic Laboratory and Louis

Katz of the Mississippi Valley Regional Blood Center for assistance in conducting the immunoassays.

This work was supported by the Department of Pathology at the University of Iowa. D.W.B. was supported by NIH T32 AI007511. K.R. and H.A.V.E. were supported by NIH T32GM007337. H.A.V.E. and N.R. were supported by NIH R01AI134733 and R21 AI144215 to W.M. The funders had no role in study design, data collection and interpretation, or the decision to submit the work for publication. All corresponding authors had full access to all the data in the study and had final responsibility for the decision to submit the manuscript for publication.

## REFERENCES

- Shang B, Wang XY, Yuan JW, Vabret A, Wu XD, Yang RF, Tian L, Ji YY, Deubel V, Sun B. 2005. Characterization and application of monoclonal antibodies against N protein of SARS-coronavirus. *Biochem Biophys Res Commun* 336:110–117. <https://doi.org/10.1016/j.bbrc.2005.08.032>.
- Walls AC, Park YJ, Tortorici MA, Wall A, McGuire AT, Velesler D. 2020. Structure, function, and antigenicity of the SARS-CoV-2 spike glycoprotein. *Cell* 181:281–292.E286. <https://doi.org/10.1016/j.cell.2020.02.058>.
- Hoffmann M, Kleine-Weber H, Pohlmann S. 2020. A multibasic cleavage site in the spike protein of SARS-CoV-2 is essential for infection of human lung cells. *Mol Cell* 78:779–784.E775. <https://doi.org/10.1016/j.molcel.2020.04.022>.
- Wrapp D, Wang N, Corbett KS, Goldsmith JA, Hsieh CL, Abiona O, Graham BS, McLellan JS. 2020. Cryo-EM structure of the 2019-nCoV spike in the prefusion conformation. *Science* 367:1260–1263. <https://doi.org/10.1126/science.abb2507>.
- Hoffmann M, Kleine-Weber H, Schroeder S, Kruger N, Herrler T, Erichsen S, Schiergens TS, Herrler G, Wu NH, Nitsche A, Muller MA, Drosten C, Pohlmann S. 2020. SARS-CoV-2 cell entry depends on ACE2 and TMPRSS2 and is blocked by a clinically proven protease inhibitor. *Cell* 181:271–280.E278. <https://doi.org/10.1016/j.cell.2020.02.052>.
- Tang T, Jaimes JA, Bidon MK, Straus MR, Daniel S, Whittaker GR. 2021. Proteolytic activation of SARS-CoV-2 spike at the S1/S2 boundary: potential role of proteases beyond furin. *ACS Infect Dis* 7:264–272. <https://doi.org/10.1021/acscinfecdis.0c00701>.
- Cao Y, Su B, Guo X, Sun W, Deng Y, Bao L, Zhu Q, Zhang X, Zheng Y, Geng C, Chai X, He R, Li X, Lv Q, Zhu H, Deng W, Xu Y, Wang Y, Qiao L, Tan Y, Song L, Wang G, Du X, Gao N, Liu J, Xiao J, Su XD, Du Z, Feng Y, Qin C, Qin C, Jin R, Xie XS. 2020. Potent neutralizing antibodies against SARS-CoV-2 identified by high-throughput single-cell sequencing of convalescent patients' B cells. *Cell* 182:73–84.E16. <https://doi.org/10.1016/j.cell.2020.05.025>.
- Wu Y, Wang F, Shen C, Peng W, Li D, Zhao C, Li Z, Li S, Bi Y, Yang Y, Gong Y, Xiao H, Fan Z, Tan S, Wu G, Tan W, Lu X, Fan C, Wang Q, Liu Y, Zhang C, Qi J, Gao GF, Gao F, Liu L. 2020. A noncompeting pair of human neutralizing antibodies block COVID-19 virus binding to its receptor ACE2. *Science* 368:1274–1278. <https://doi.org/10.1126/science.abc2241>.
- Zhou X, Ma F, Xie J, Yuan M, Li Y, Shaabani N, Zhao F, Huang D, Wu NC, Lee CD, Liu H, Li J, Chen Z, Hong Y, Liu WH, Xiao N, Burton DR, Tu H, Li H, Chen X, Tejjaro JR, Wilson IA, Xiao C, Huang Z. 2021. Diverse immunoglobulin gene usage and convergent epitope targeting in neutralizing antibody responses to SARS-CoV-2. *Cell Rep* 35:109109. <https://doi.org/10.1016/j.celrep.2021.109109>.
- Brouwer PJM, Daniels TG, van der Straten K, Snitselaar JL, Aldon Y, Bangaru S, Torres JL, Okba NMA, Claireaux M, Kerster G, Bentlage AEH, van Haaren MM, Guerra D, Burger JA, Schermer EE, Verheul KD, van der Velde N, van der Kooij A, van Schooten J, van Breemen MJ, Bijl TPL, Slieden K, Aartse A, Derking R, Bontjer I, Kootstra NA, Wiersinga WJ, Vidarsson G, Haagmans BL, Ward AB, de Bree GJ, Sanders RW, van Gils MJ. 2020. Potent neutralizing antibodies from COVID-19 patients define multiple targets of vulnerability. *Science* 369:643–650. <https://doi.org/10.1126/science.abc5902>.
- Cerutti G, Guo Y, Zhou T, Gorman J, Lee M, Rapp M, Reddem ER, Yu J, Bahna F, Bimela J, Huang Y, Katsamba PS, Liu L, Nair MS, Rawi R, Olia AS, Wang P, Zhang B, Chuang GY, Ho DD, Sheng Z, Kwong PD, Shapiro L. 2021. Potent SARS-CoV-2 neutralizing antibodies directed against spike N-terminal domain target a single supersite. *Cell Host Microbe* 29:819–833.E817. <https://doi.org/10.1016/j.chom.2021.03.005>.
- Robbiani DF, Gaebler C, Muecksch F, Lorenzi JCC, Wang Z, Cho A, Agudelo M, Barnes CO, Gazumyan A, Finkin S, Hagglof T, Oliveira TY, Viant C, Hurley A, Hoffmann HH, Millard KG, Kost RG, Cipolla M, Gordon K, Bianchini F, Chen ST, Ramos V, Patel R, Dizon J, Shimeliovich I, Mendoza P, Hartweg H, Nogueira L, Pack M, Horowitz J, Schmidt F, Weisblum Y, Michailidis E, Ashbrook AW, Waltari E, Pak JE, Huey-Tubman KE, Koranda N, Hoffman PR, West AP, Jr, Rice CM, Hatziioannou T, Bjorkman PJ, Bieniasz PD, Caskey M, Nussenzweig MC. 2020. Convergent antibody responses to SARS-CoV-2 in convalescent individuals. *Nature* 584:437–442. <https://doi.org/10.1038/s41586-020-2456-9>.
- Zhou D, Dejnirattisai W, Supasa P, Liu C, Mentzer AJ, Ginn HM, Zhao Y, Duyvesteyn HME, Tuekprakhon A, Nutalai R, Wang B, Paesen GC, Lopez-Camacho C, Slon-Campos J, Hallis B, Coombes N, Bewley K, Charlton S, Walter TS, Skelly D, Lumley SF, Dold C, Levin R, Dong T, Pollard AJ, Knight JC, Crook D, Lambe T, Clutterbuck E, Bibi S, Flaxman A, Bittaye M, Bellij-Rammerstorfer S, Gilbert S, James W, Carroll MW, Klenerman P, Barnes E, Dunachie SJ, Fry EE, Mongkolsapaya J, Ren J, Stuart DI, Screaton GR. 2021. Evidence of escape of SARS-CoV-2 variant B.1.351 from natural and vaccine-induced sera. *Cell* 184:2348–2361.E2346. <https://doi.org/10.1016/j.cell.2021.02.037>.
- Zost SJ, Gilchuk P, Chen RE, Case JB, Reidy JX, Trivette A, Nargi RS, Sutton RE, Suryadevara N, Chen EC, Binshtein E, Shrihari S, Ostrowski M, Chu HY, Didier JE, MacRenaris KW, Jones T, Day S, Myers L, Eun-Hyung Lee F, Nguyen DC, Sanz I, Martinez DR, Rothlauf PW, Bloyet LM, Whelan SPJ, Baric RS, Thackray LB, Diamond MS, Carnahan RH, Crowe JE, Jr. 2020. Rapid isolation and profiling of a diverse panel of human monoclonal antibodies targeting the SARS-CoV-2 spike protein. *Nat Med* 26:1422–1427. <https://doi.org/10.1038/s41591-020-0998-x>.
- Dogan M, Kozhaya L, Placek L, Gunter C, Yigit M, Hardy R, Plassmeyer M, Coatney P, Lillard K, Bukhari Z, Kleinberg M, Hayes C, Arditi M, Klapper E, Merin N, Liang BT, Gupta R, Alpan O, Unutmaz D. 2021. SARS-CoV-2 specific antibody and neutralization assays reveal the wide range of the humoral immune response to virus. *Commun Biol* 4:129. <https://doi.org/10.1038/s42003-021-01649-6>.
- Chi X, Yan R, Zhang J, Zhang G, Zhang Y, Hao M, Zhang Z, Fan P, Dong Y, Yang Y, Chen Z, Guo Y, Zhang J, Li Y, Song X, Chen Y, Xia L, Fu L, Hou L, Xu J, Yu C, Li J, Zhou Q, Chen W. 2020. A neutralizing human antibody binds to the N-terminal domain of the spike protein of SARS-CoV-2. *Science* 369:650–655. <https://doi.org/10.1126/science.abc6952>.
- Suryadevara N, Shrihari S, Gilchuk P, VanBlargan LA, Binshtein E, Zost SJ, Nargi RS, Sutton RE, Winkler ES, Chen EC, Fouch ME, Davidson E, Doranz BJ, Chen RE, Shi PY, Carnahan RH, Thackray LB, Diamond MS, Crowe JE, Jr. 2021. Neutralizing and protective human monoclonal antibodies recognizing the N-terminal domain of the SARS-CoV-2 spike protein. *Cell* 184:2316–2331.E2315. <https://doi.org/10.1016/j.cell.2021.03.029>.
- Wang N, Sun Y, Feng R, Wang Y, Guo Y, Zhang L, Deng YQ, Wang L, Cui Z, Cao L, Zhang YJ, Li W, Zhu FC, Qin CF, Wang X. 2021. Structure-based development of human antibody cocktails against SARS-CoV-2. *Cell Res* 31:101–103. <https://doi.org/10.1038/s41422-020-00446-w>.
- Shah P, Canziani GA, Carter EP, Chaiken I. 2021. The case for S2: the potential benefits of the S2 subunit of the SARS-CoV-2 spike protein as an immunogen in fighting the COVID-19 pandemic. *Front Immunol* 12:637651. <https://doi.org/10.3389/fimmu.2021.637651>.
- Nguyen-Contant P, Embong AK, Kanagaiah P, Chaves FA, Yang H, Branche AR, Topham DJ, Sangster MY. 2020. S protein-reactive IgG and memory B cell production after human SARS-CoV-2 infection includes broad reactivity to the S2 subunit. *mBio* 11:e01991–20. <https://doi.org/10.1128/mBio.01991-20>.
- Steffen HA, Swartz SR, Jackson JB, Kenne KA, Ten Eyck PP, Merryman AS, Castaneda CN, Marsden K, Maxwell T, Merrill AE, Krasowski MD, Rysavy MB. 2021. SARS-CoV-2 infection during pregnancy in a rural Midwest all-delivery cohort and associated maternal and neonatal outcomes. *Am J Perinatol* 38:614–621. <https://doi.org/10.1055/s-0041-1723938>.

22. Salimi H, Johnson J, Flores MG, Zhang MS, O'Malley Y, Houtman JC, Schlievert PM, Haim H. 2020. The lipid membrane of HIV-1 stabilizes the viral envelope glycoproteins and modulates their sensitivity to antibody neutralization. *J Biol Chem* 295:348–362. <https://doi.org/10.1074/jbc.RA119.009481>.
23. Johnson J, Flores MG, Rosa J, Han C, Salvi AM, DeMali KA, Jagnow JR, Sparks A, Haim H. 2020. The high content of fructose in human semen competitively inhibits broad and potent antivirals that target high-mannose glycans. *J Virol* 94:e01749-19. <https://doi.org/10.1128/JVI.01749-19>.
24. Johnson J, Zhai Y, Salimi H, Espy N, Eichelberger N, DeLeon O, O'Malley Y, Courter J, Smith AB, 3rd, Madani N, Sodroski J, Haim H. 2017. Induction of a tier-1-like phenotype in diverse tier-2 isolates by agents that guide HIV-1 Env to perturbation-sensitive, nonnative states. *J Virol* 91:e00174-17. <https://doi.org/10.1128/JVI.00174-17>.
25. Amanat F, Thapa M, Lei T, Ahmed SMS, Adelsberg DC, Carreno JM, Strohmeier S, Schmitz AJ, Zafar S, Zhou JQ, Rijnink W, Alshammary H, Borchering N, Reiche AG, Srivastava K, Sordillo EM, van Bakel H, Turner JS, Bajic G, Simon V, Ellebedy AH, Krammer F, Personalized Virology Initiative. 2021. The plasmablast response to SARS-CoV-2 mRNA vaccination is dominated by non-neutralizing antibodies that target both the NTD and the RBD. *medRxiv*. <https://www.medrxiv.org/content/10.1101/2021.03.07.21253098>.
26. Liu L, Wang P, Nair MS, Yu J, Rapp M, Wang Q, Luo Y, Chan JF, Sahi V, Figueroa A, Guo XV, Cerutti G, Bimela J, Gorman J, Zhou T, Chen Z, Yuen KY, Kwong PD, Sodroski JG, Yin MT, Sheng Z, Huang Y, Shapiro L, Ho DD. 2020. Potent neutralizing antibodies against multiple epitopes on SARS-CoV-2 spike. *Nature* 584:450–456. <https://doi.org/10.1038/s41586-020-2571-7>.
27. Jungbauer C, Weseslindtner L, Weidner L, Gansdorfer S, Farcet MR, Gschaider-Reichhart E, Kreil TR. 2021. Characterization of 100 sequential SARS-CoV-2 convalescent plasma donations. *Transfusion* 61:12–16. <https://doi.org/10.1111/trf.16119>.
28. Brochet E, Demey B, Touze A, Belouzard S, Dubuisson J, Schmit JL, Duverlie G, Francois C, Castelain S, Helle F. 2020. Anti-spike, anti-nucleocapsid and neutralizing antibodies in SARS-CoV-2 inpatients and asymptomatic individuals. *Front Microbiol* 11:584251. <https://doi.org/10.3389/fmicb.2020.584251>.
29. Gniadek TJ, Thiede JM, Matchett WE, Gress AR, Pape KA, Fiege JK, Jenkins MK, Menachery VD, Langlois RA, Bold TD. 2021. SARS-CoV-2 neutralization and serology testing of COVID-19 convalescent plasma from donors with nonsevere disease. *Transfusion* 61:17–23. <https://doi.org/10.1111/trf.16101>.
30. Case JB, Rothlauf PW, Chen RE, Liu Z, Zhao H, Kim AS, Bloyet LM, Zeng Q, Tahan S, Droit L, Ilagan MXG, Tartell MA, Amarasinghe G, Henderson JP, Miersch S, Ustav M, Sidhu S, Virgin HW, Wang D, Ding S, Corti D, Theel ES, Fremont DH, Diamond MS, Whelan SPJ. 2020. Neutralizing antibody and soluble ACE2 inhibition of a replication-competent VSV-SARS-CoV-2 and a clinical isolate of SARS-CoV-2. *Cell Host Microbe* 28:475–485.E475. <https://doi.org/10.1016/j.chom.2020.06.021>.
31. Klein SL, Pekosz A, Park HS, Ursin RL, Shapiro JR, Benner SE, Littlefield K, Kumar S, Naik HM, Betenbaugh MJ, Shrestha R, Wu AA, Hughes RM, Burgess I, Caturegli P, Laeyendecker O, Quinn TC, Sullivan D, Shoham S, Redd AD, Bloch EM, Casadevall A, Tobian AA. 2020. Sex, age, and hospitalization drive antibody responses in a COVID-19 convalescent plasma donor population. *J Clin Invest* 130:6141–6150. <https://doi.org/10.1172/JCI142004>.
32. Solastie A, Virta C, Haveri A, Ekstrom N, Kantele A, Miettinen S, Lempainen J, Jalkanen P, Kakkola L, Dub T, Julkunen I, Melin M. 2021. A highly sensitive and specific SARS-CoV-2 spike- and nucleoprotein-based fluorescent multiplex immunoassay (FMIA) to measure IgG, IgA, and IgM class antibodies. *Microbiol Spectr* 9:e01131-21. <https://doi.org/10.1128/Spectrum.01131-21>.
33. Berger Rentsch M, Zimmer G. 2011. A vesicular stomatitis virus replicon-based bioassay for the rapid and sensitive determination of multi-species type I interferon. *PLoS One* 6:e25858. <https://doi.org/10.1371/journal.pone.0025858>.
34. Muecksch F, Wise H, Batchelor B, Squires M, Semple E, Richardson C, McGuire J, Clearly S, Furrie E, Greig N, Hay G, Templeton K, Lorenzi JCC, Hatziioannou T, Jenks S, Bieniasz PD. 2021. Longitudinal serological analysis and neutralizing antibody levels in coronavirus disease 2019 convalescent patients. *J Infect Dis* 223:389–398. <https://doi.org/10.1093/infdis/jiaa659>.
35. Patel EU, Bloch EM, Clarke W, Hsieh YH, Boon D, Eby Y, Fernandez RE, Baker OR, Keruly M, Kirby CS, Klock E, Littlefield K, Miller J, Schmidt HA, Sullivan P, Pivowar-Manning E, Shrestha R, Redd AD, Rothman RE, Sullivan D, Shoham S, Casadevall A, Quinn TC, Pekosz A, Tobian AAR, Laeyendecker O. 2021. Comparative performance of five commercially available serologic assays to detect antibodies to SARS-CoV-2 and identify individuals with high neutralizing titers. *J Clin Microbiol* 59:e02257-20. <https://doi.org/10.1128/JCM.02257-20>.
36. Tang MS, Case JB, Franks CE, Chen RE, Anderson NW, Henderson JP, Diamond MS, Gronowski AM, Farnsworth CW. 2020. Association between SARS-CoV-2 neutralizing antibodies and commercial serological assays. *Clin Chem* 66:1538–1547. <https://doi.org/10.1093/clinchem/hvaa211>.
37. Amanat F, Thapa M, Lei T, Ahmed SMS, Adelsberg DC, Carreño JM, Strohmeier S, Schmitz AJ, Zafar S, Zhou JQ, Rijnink W, Alshammary H, Borchering N, Reiche AG, Srivastava K, Sordillo EM, van Bakel H, Turner JS, Bajic G, Simon V, Ellebedy AH, Krammer F, Ahmed B, Altman D, Amoako A, Awawda M, Beach K, Bermúdez-González C, Chernet R, Eaker L, Fabre S, Ferreri ED, Floda D, Gleason C, Kleiner G, Jurczyszak D, Matthews J, Mendez W, Mulder LCF, Polanco J, Russo K, Salimbangon A, Saksena M, Shin AS, Sominsky L, Suthakaran S, Wajnberg A. 2021. SARS-CoV-2 mRNA vaccination induces functionally diverse antibodies to NTD, RBD, and S2. *Cell* 184:3936–3948.E10. <https://doi.org/10.1016/j.cell.2021.06.005>.
38. Voss WN, Hou YJ, Johnson NV, Delidakis G, Kim JE, Javanmardi K, Horton AP, Bartzoka F, Paresi CJ, Tanno Y, Chou CW, Abbasi SA, Pickens W, George K, Boutz DR, Towers DM, McDaniel JR, Billick D, Goike J, Rowe L, Batra D, Pohl J, Lee J, Gangappa S, Sambhara S, Gadush M, Wang N, Person MD, Iverson BL, Gollihar JD, Dye JM, Herbert AS, Finkelstein IJ, Baric RS, McLellan JS, Georgiou G, Lavinder JJ, Ippolito GC. 2021. Prevalent, protective, and convergent IgG recognition of SARS-CoV-2 non-RBD spike epitopes. *Science* 372:1108–1112. <https://doi.org/10.1126/science.abg5268>.
39. Niu L, Wittrock KN, Clabaugh GC, Srivastava V, Cho MW. 2021. A structural landscape of neutralizing antibodies against SARS-CoV-2 receptor binding domain. *Front Immunol* 12:647934. <https://doi.org/10.3389/fimmu.2021.647934>.
40. Seydoux E, Homad LJ, MacCamy AJ, Parks KR, Hurlburt NK, Jennewein MF, Akins NR, Stuart AB, Wan YH, Feng J, Whaley RE, Singh S, Boeckh M, Cohen KW, McElrath MJ, Englund JA, Chu HY, Pancera M, McGuire AT, Stamataatos L. 2020. Analysis of a SARS-CoV-2-infected individual reveals development of potent neutralizing antibodies with limited somatic mutation. *Immunity* 53:98–105.e105. <https://doi.org/10.1016/j.immuni.2020.06.001>.
41. Collier DA, De Marco A, Ferreira I, Meng B, Datt RP, Walls AC, Kemp SA, Bassi J, Pinto D, Silacci-Fregni C, Bianchi S, Tortorici MA, Bowen J, Culap K, Jaconi S, Cameroni E, Snell G, Pizzuto MS, Pellanda AF, Garzoni C, Riva A, Collaboration C-N, - Elmer A, Kingston N, Graves B, McCoy LE, Smith KGC, Bradley JR, Temperton N, Ceron-Gutierrez L, Barcenas-Morales G, Consortium C-GU, Harvey W, Virgin HW, Lanzavecchia A, Piccoli L, Doffinger R, Willis M, Veeler D, Corti D, Gupta RK, COVID-19 Genomics UK (COG-UK) Consortium. 2021. Sensitivity of SARS-CoV-2 B.1.1.7 to mRNA vaccine-elicited antibodies. *Nature* 593:136–141. <https://doi.org/10.1038/s41586-021-03412-7>.
42. Tada T, Zhou H, Dcosta BM, Samanovic MI, Mulligan MJ, Landau NR. 2021. Partial resistance of SARS-CoV-2 Delta variants to vaccine-elicited antibodies and convalescent sera. *iScience* 24:103341. <https://doi.org/10.1016/j.isci.2021.103341>.
43. Wang B, Goh YS, Fong SW, Young BE, Ngoh EZX, Chavatte JM, Salleh SNM, Yeo NK, Amrun SN, Hor PX, Loh CY, Lee CY, Chan YH, Chang ZW, Tay MZ, Routers A, Torres-Ruesta A, Carissimo G, Soh MK, Lee RTM, Xu Y, Pada S, Lin RTP, Leo YS, Lye DC, Maurer-Stroh S, Ng LFP, Renia L, Wang CI. 2021. Resistance of SARS-CoV-2 Delta variant to neutralization by BNT162b2-elicited antibodies in Asians. *Lancet Reg Health West Pac* 15:100276. <https://doi.org/10.1016/j.lanwpc.2021.100276>.
44. Zhang L, Li Q, Liang Z, Li T, Liu S, Cui Q, Nie J, Wu Q, Qu X, Huang W, Wang Y. 2022. The significant immune escape of pseudotyped SARS-CoV-2 variant Omicron. *Emerg Microbes Infect* 11:1–5. <https://doi.org/10.1080/22221751.2021.2017757>.
45. Jaaskelainen AJ, Kuivaniemi S, Kekalainen E, Ahava MJ, Loginov R, Kallio-Kokko H, Vapalahti O, Jarva H, Kurkela S, Lappalainen M. 2020. Performance of six SARS-CoV-2 immunoassays in comparison with microneutralization. *J Clin Virol* 129:104512. <https://doi.org/10.1016/j.jcv.2020.104512>.
46. Luchsinger LL, Ransegnola B, Jin D, Muecksch F, Weisblum Y, Bao W, George PJ, Rodriguez M, Tricoche N, Schmidt F, Gao C, Jawahar S, Pal M, Schnall E, Zhang H, Strauss D, Yazdanbakhsh K, Hillyer CD, Bieniasz PD, Hatziioannou T. 2020. Serological assays estimate highly variable SARS-CoV-2 neutralizing antibody activity in recovered COVID-19 patients. *J Clin Microbiol* 58:e02005-20. <https://doi.org/10.1128/JCM.02005-20>.

47. Grenache DG, Ye C, Bradfute SB. 2021. Correlation of SARS-CoV-2 neutralizing antibodies to an automated chemiluminescent serological immunoassay. *J Appl Lab Med* 6:491–495. <https://doi.org/10.1093/jalm/jfaa195>.
48. Rychert J, Couturier MR, Elgort M, Lozier BK, La'ulu S, Genzen JR, Straseski JA, Delgado JC, Slev PR. 2021. Evaluation of three SARS CoV-2 IgG antibody assays and correlation with neutralizing antibodies. *J Appl Lab Med* 6:614–624. <https://doi.org/10.1093/jalm/jfaa188>.
49. Haim H, Salas I, Sodroski J. 2013. Proteolytic processing of the human immunodeficiency virus envelope glycoprotein precursor decreases conformational flexibility. *J Virol* 87:1884–1889. <https://doi.org/10.1128/JVI.02765-12>.
50. Kong L, Sheppard NC, Stewart-Jones GBE, Robson CL, Chen H, Xu X, Krashias G, Bonomelli C, Scanlan CN, Kwong PD, Jeffs SA, Jones IM, Sattentau QJ. 2010. Expression-system-dependent modulation of HIV-1 envelope glycoprotein antigenicity and immunogenicity. *J Mol Biol* 403:131–147. <https://doi.org/10.1016/j.jmb.2010.08.033>.
51. Raska M, Takahashi K, Czernekova L, Zachova K, Hall S, Moldoveanu Z, Elliott MC, Wilson L, Brown R, Jancova D, Barnes S, Vrbkova J, Tomana M, Smith PD, Mestecky J, Renfrow MB, Novak J. 2010. Glycosylation patterns of HIV-1 gp120 depend on the type of expressing cells and affect antibody recognition. *J Biol Chem* 285:20860–20869. <https://doi.org/10.1074/jbc.M109.085472>.
52. Huang C, Tan Z, Zhao K, Zou W, Wang H, Gao H, Sun S, Bu D, Chai W, Li Y. 2021. The effect of N-glycosylation of SARS-CoV-2 spike protein on the virus interaction with the host cell ACE2 receptor. *iScience* 24:103272. <https://doi.org/10.1016/j.isci.2021.103272>.
53. Wang C, van Haperen R, Gutierrez-Alvarez J, Li W, Okba NMA, Albuilescu I, Widjaja I, van Dieren B, Fernandez-Delgado R, Sola I, Hurdiss DL, Daramola O, Grosveld F, van Kuppeveld FJM, Haagmans BL, Enjuanes L, Drabek D, Bosch BJ. 2021. A conserved immunogenic and vulnerable site on the coronavirus spike protein delineated by cross-reactive monoclonal antibodies. *Nat Commun* 12:1715. <https://doi.org/10.1038/s41467-021-21968-w>.
54. Chen HY, Huang C, Tian L, Huang X, Zhang C, Llewellyn GN, Rogers GL, Andresen K, O'Gorman MRG, Chen YW, Cannon PM. 2021. Cytoplasmic tail truncation of SARS-CoV-2 spike protein enhances titer of pseudotyped vectors but masks the effect of the D614G mutation. *J Virol* 95:e00966-21. <https://doi.org/10.1128/JVI.00966-21>.
55. Cervera L, Gonzalez-Dominguez I, Segura MM, Godia F. 2017. Intracellular characterization of Gag VLP production by transient transfection of HEK 293 cells. *Biotechnol Bioeng* 114:2507–2517. <https://doi.org/10.1002/bit.26367>.